The EMBO Journal Vol.16 No.17 pp.5162–5177, 1997

Molecular recognition of human angiogenin by placental ribonuclease inhibitor—an X-ray crystallographic study at 2.0 Å resolution

Anastassios C.Papageorgiou[1], Robert Shapiro[2,3] and K.Ravi Acharya[1,4]

[1]Department of Biology and Biochemistry, University of Bath, Claverton Down, Bath BA2 7AY, UK, [2]Center for Biochemical and Biophysical Sciences and Medicine and [3]Department of Pathology, Harvard Medical School, Boston, MA 02115, USA

[4]Corresponding author
e-mail: K.R.Acharya@bath.ac.uk

Human placental RNase inhibitor (hRI), a leucine-rich repeat protein, binds the blood vessel-inducing protein human angiogenin (Ang) with extraordinary affinity (K_i <1 fM). Here we report a 2.0 Å resolution crystal structure for the hRI–Ang complex that, together with extensive mutagenesis data from earlier studies, reveals the molecular features of this tight interaction. The hRI–Ang binding interface is large and encompasses 26 residues from hRI and 24 from Ang, recruited from multiple domains of both proteins. However, a substantial fraction of the energetically important contacts involve only a single region of each: the C-terminal segment 434–460 of hRI and the ribonucleolytic active centre of Ang, most notably the catalytic residue Lys40. Although the overall docking of Ang resembles that observed for RNase A in the crystal structure of its complex with the porcine RNase inhibitor, the vast majority of the interactions in the two complexes are distinctive, indicating that the broad specificity of the inhibitor for pancreatic RNase superfamily proteins is based largely on its capacity to recognize features unique to each of them. The implications of these findings for the development of small, hRI-based inhibitors of Ang for therapeutic use are discussed.

Keywords: angiogenin/epitope mapping/molecular recognition/ribonuclease inhibitor/X-ray crystallography

Introduction

The molecular basis for protein–protein recognition, a critical issue in structural biology, recently has come under intense scrutiny. A large number of crystal structures of protein–protein complexes have now been determined, and considerable progress has been made toward an understanding of their general characteristics (Janin and Chothia, 1990; Jones and Thornton, 1996). Nonetheless, it has not yet become possible to deduce the energetic contributions of individual interface residues based solely on crystallography. Moreover, in the few instances where detailed functional information on a protein–protein interaction has also been collected by site-specific mutagenesis, some residues 'observed' to form strong contacts in the crystal structures have been found to have little functional importance, and other residues have been shown to make strong contributions that were not apparent from the structures (as discussed by Clackson and Wells, 1995; Schreiber and Fersht, 1995; Chen and Shapiro, 1997). Examination of additional complexes by an approach that combines structural and functional data should lead to a more predictive understanding of the physicochemical basis for protein–protein recognition.

The complex of human placental RNase inhibitor (hRI), a 50 kDa leucine-rich repeat protein, with human angiogenin (Ang), a 14.1 kDa blood vessel-inducing protein in the pancreatic RNase superfamily (Fett *et al.*, 1985; Strydom *et al.*, 1985), is among the tightest on record (K_i <1 fM; Lee *et al.*, 1989a). Binding of hRI inhibits both the enzymatic and angiogenic activities of Ang (Shapiro and Vallee, 1987); indeed this finding provided one of the first indications that the ribonucleolytic action of Ang is required for its biological activity, as later confirmed by mutational studies (Shapiro and Vallee, 1989; Shapiro *et al.*, 1989). The detailed mechanism of Ang action and the identity of its *in vivo* substrate in particular remain to be determined. However, Ang has been demonstrated to interact with endothelial cells in a variety of ways pertinent to angiogenesis: it (i) binds cell surface receptors, producing a mitogenic response (Hu *et al.*, 1997); (ii) induces second messengers (Bicknell and Vallee, 1988, 1989); (iii) stimulates cell-associated proteolytic activity and invasiveness (Hu *et al.*, 1994); (iv) mediates cell adhesion (Soncin, 1992); and (v) organizes cells into tubular structures (Jimi *et al.*, 1995). Moreover, Ang undergoes nuclear translocation in these cells (Moroianu and Riordan, 1994), bringing it in direct apposition to potential RNA substrates.

Ang originally was isolated from human adenocarcinoma cell conditioned medium, and recent studies indicate that it is critically involved in the establishment and growth of a wide range of human tumour types in athymic mice (Olson *et al.*, 1994, 1995; Olson and Fett, 1996). These results identify Ang as a potentially useful target for new anticancer drugs. hRI itself is unlikely to have therapeutic utility, primarily because of its sensitivity to oxidation (Blackburn *et al.*, 1977) and its broad specificity for proteins in the pancreatic RNase superfamily (see Lee and Vallee, 1993; Hofsteenge, 1997). hRI binds human RNase-2 [also known as placental RNase and eosinophil-derived neurotoxin (EDN)] almost as avidly as it binds Ang (Shapiro and Vallee, 1991), and K_i values for pancreatic-type RNases are still in the mid to upper femtomolar range [44 fM for bovine (Lee *et al.*, 1989a) and 200 fM for human (Boix *et al.*, 1996)]. The interactions of hRI with yet other RNases [human RNase-4 (Shapiro *et al.*, 1986) and RNase-6 (R.Shapiro, unpublished observations)] are also very tight, although in these cases the dissociation constants have not been quantitated. The high affinity of hRI for all of its ligands is remarkable in view of the fact that these proteins share only ~25–35% sequence identity.

We report now a crystal structure for the hRI–Ang complex at 2.0 Å resolution. This structure, in combination with extensive functional data on the complex available from earlier studies, provides a detailed view of how Ang and hRI form their extremely strong association. Although the overall docking of Ang resembles that observed for RNase A in the crystal structure of its complex with the closely related porcine RNase inhibitor (pRI) (Kobe and Deisenhofer, 1995), the specific interactions at the interface differ substantially. Indeed, the vast majority of the hydrogen bonds and van der Waals contacts in the two complexes are distinctive, indicating that inhibitor versatility is based in large part on its capacity to recognize features unique to each of its ligands. This information should now provide a basis for efforts to design small, active hRI derivatives or mimics suitable for therapeutic use.

Results

Crystallization of the hRI–Ang complex

Ionic interactions have been shown to play an important role in the binding of both Ang and RNase A to hRI (Lee *et al.*, 1989a,b; Chen and Shapiro, 1997). Therefore, relatively low ionic strength was maintained in crystallization solutions and non-ionic precipitants were used. Concentrations of phosphate and sulfate in particular were held low since these bind to the active sites of pancreatic RNase family proteins (Richards and Wyckoff, 1973; Shapiro *et al.*, 1987; Howlin *et al.*, 1989; Mosimann *et al.*, 1996). Crystals of the hRI–Ang complex were grown by pre-forming the complex in HEPES buffer, and then adding an equal volume of a reservoir solution containing citrate, a small amount of ammonium sulfate and polyethylene glycol (PEG) as the precipitant (see Materials and methods). The stability of the complex under these conditions [but with 0.1 mM rather than 25 mM dithiothreitol (DTT)] was evaluated by measuring the rate constant for its dissociation. For this purpose, [^{14}C]Ang was used and the reservoir solution contained a large molar excess of RNase A to act as a scavenger for any free RI dissociating from the complex (Chen and Shapiro, 1997). At various times, free and RI-bound [^{14}C]Ang were separated and quantitated by scintillation counting. After 4 days at 25°C, <2% of the Ang had been released, indicating that the rate of complex dissociation was similar to that measured under the standard conditions used for kinetic studies ($t_{1/2}$ = 70 days).

Description of overall structure

The three-dimensional crystal structure of the hRI–Ang complex was determined at 2.0 Å resolution (Figure 1, Table I). The complex crystallizes as a dimer (Figure 2A), although in solution it probably exists as a monomer, as has been shown for free hRI and its complex with RNase A (Blackburn *et al.*, 1977). The two monomers have nearly identical structures [the r.m.s. deviations are 0.26 Å (C^α atoms), 0.56 Å (main-chain) and 0.96 Å (side-chain)]. The interactions detailed below are those in molecule 1, and can be assumed to be replicated in molecule 2 except where noted otherwise. The dimer contains 133 ordered water molecules (76 in molecule 1 and 57 in molecule 2); the majority either lie at the monomer–monomer interface or mediate interactions between Ang and hRI. No sulfate or other salt molecules from the crystallization solution are observed in the structure.

The topology of the hRI molecule is closely similar to that of pRI (Kobe and Deisenhofer, 1993, 1995) (Figure 2B). The two proteins exhibit 77% amino acid sequence identity and one-third of the substitutions are conservative (Figure 3). Compared with the porcine protein, hRI has a four residue extension at the N-terminus, and no insertions or deletions. The secondary structural features of the two proteins are nearly identical. Briefly, the 15 alternating 29 and 28 residue leucine-rich repeat units that comprise most of the hRI molecule form β–α hairpin units and are arranged in the non-globular, symmetric shape of a horseshoe (Figure 2A and B). The inner and outer diameters of the horseshoe are ~20 and 68 Å, respectively, and its thickness is 35 Å (the corresponding values for the pRI complex are 21, 67 and 32 Å). The molecular fold is generated by an extended right-handed superhelix with alternating β-strands and α-helices. All of the 17 short β-strands, which form a solvent-exposed parallel β-sheet, line up on the inner surface of the horseshoe (except for the elongated N-terminal strand that is involved in dimerization; see below); the outer surface is decorated by 16 helices that are in most instances 10–13 residues in length. These secondary structural elements are connected by loops that contain 4–11 residues. The horseshoe structure is stabilized by a large number of intra- and inter-repeat interactions, in the same manner as described previously for free pRI (Kobe and Deisenhofer, 1993). All of the 32 hRI cysteine residues are in the reduced form and are well ordered in the complex.

Structural information is not yet available for the free hRI molecule, and it is therefore not possible to gauge what conformational changes, if any, occur upon Ang binding. However, comparison of the hRI structure in the complex with those of free and RNase A-bound pRI suggests that the type of global structural alterations associated with binding of RNase A may not occur with Ang. Kobe and Deisenhofer (1995, 1996) reported an accumulation of small shifts along the polypeptide chain in bound versus free pRI, resulting in a widening of the horseshoe opening from 12 to 14.4 Å. The corresponding distance in the hRI–Ang complex is 12.7 Å, much closer to that in free pRI. Moreover, a least-squares superposition of the hRI structure (C^α atoms) with those of free and bound pRI results in r.m.s. deviations of 1.24 and 1.88 Å, respectively (compared with 1.46 Å for free versus bound pRI), indicating that the hRI backbone structure in the Ang complex is more similar to free than to RNase A-bound pRI.

Alignment of hRI and bound pRI in segments of ~150 residues reduces the r.m.s. deviation in C^α positions to 0.63–0.87 Å. Comparison of the side-chain orientations within these segments reveals that several contact residues for Ang on hRI (see Table III below) adopt positions that differ significantly from those of the corresponding residues in the pRI complex. The largest changes are seen for Trp261 and Trp318: the indole ring of Trp261 occupies a space similar to that of the corresponding Trp in pRI (257) but is rotated by ~180°; the indoles of Trp318 and pRI Trp314 are nearly perpendicular to each other. In addition, the positions of the side-chain OH and carboxylate of the C-terminal Ser are interchanged in hRI and

Fig. 1. A view of a slice through the electron density map calculated using $2|F_{obs}|-|F_{calc}|$ coefficients and calculated phases onto the refined coordinates of the hRI–Ang complex.

pRI. Potentially significant shifts of 1–4 Å are also observed for Tyr150, Lys320, Glu344, Gln346, Glu440 and Tyr437. Numerous RI side chains, primarily flexible surface residues, outside the interface region also have different conformations in the two proteins.

The structure of Ang in the complex is similar to those of free <Glu-1 (D.D.Leonidas, S.C.Allen and K.R.Acharya, unpublished results) and Met-(–1) Ang (Acharya *et al.*, 1994). All three disulfide bridges are present and well ordered, even though the crystals were grown in the presence of 25 mM DTT. Superposition of 118 C^{α} atoms in free and complexed <Glu-1 Ang (i.e. excluding the three N-terminal and two C-terminal residues, which are disordered in both structures) results in an r.m.s. deviation of 0.78 Å. This alignment can be improved further if the loop region 58–68, which has poor electron density in the complex, is excluded from the superposition (r.m.s. deviation 0.57 Å). This segment forms part of the putative cell receptor-binding site in Ang (Hallahan *et al.*, 1991). It is better ordered in the free Ang structure, where it makes crystal packing contacts. The polypeptide chain of Ang in the complex differs from that of the free protein in two additional areas: 18–20 and 85–89. The former is highly flexible and does not contact RI. However, residues 85–89 are part of a loop that forms numerous interactions with RI through its main-chain (Gly85 and Gly86) and side-chain atoms (Pro88 and Trp89), and this movement greatly improves the complementarity of the two proteins in this region (see below). Other Ang side chains at the RI interface—Arg5, Arg24, Arg31, Arg32, Asp41, Arg95 and Glu108—also adopt conformations that differ appreciably from those in the free structure, with distances between the corresponding atoms in the two structures ranging from 2 to 6 Å. Thus binding of Ang to RI involves more extensive rearrangement of the interface region than was observed for RNase A, where only Lys7, Arg39, Asn67, Gln69 and Lys91 display comparable changes in the bound versus free structures.

Table I. Crystallographic data processing and refinement statistics

Space group monoclinic, $P2_1$	
Cell dimensions	a = 66.55 Å, b = 105.60 Å, c = 93.52 Å, β = 107.09°
Two hRI–hAng complex molecules/a.u. (solvent content ~51%)	
Resolution (Å)	40.0–2.0
N_m[a]	158 593
N_u[b]	72 355
Overall completeness (%)	86.9
$<I/\sigma(I)>$ (average)	4.5 (1.6 between 2.07–2.0Å)
Completeness of outer shell	65.4% (2.07–2.0 Å)
R_{sym}[c] (%)	9.4
No. of reflections used in refinement (20–2 Å)	72 308
R_{cryst}[d] ($F>0\sigma$) (%)	19.3
R_{free}[e] (%)	28.6
No. of protein atoms	8806
No. of water molecules	133
R.m.s deviation in bond lengths (Å)	0.009
bond angles (°)	1.40
Average *B*-factors (Å^2)	
Overall *B*-factor (Wilson plot)	40.4
hRI–hAng molecule 1	41.2
hRI–hAng molecule 2	42.6
hRI all atoms	40.4 mol 1 41.2 mol 2
main-chain atoms	37.5 mol 1 39.2 mol 2
side-chain atoms	43.7 mol 1 45.3 mol 2
Ang all atoms	44.1 mol 1 45.1 mol 2
main-chain atoms	41.7 mol 1 42.5 mol 2
side-chain atoms	46.5 mol 1 47.6 mol 2
Water molecules	42.2

[a]Number of measurements.
[b]Number of unique reflections.
[c]$R_{sym} = \Sigma_{hkl}\Sigma_i|I_i(hkl)-<I(hkl)>|/\Sigma_{hkl}\Sigma_i I_i(hkl)$ where $<I>$ is the averaged intensity of the i observations of reflection hkl.
[d]$R_{cryst} = \Sigma||F_o|-|F_c||/\Sigma|F_o|$ where F_o and F_c are the observed and calculated structure factor amplitudes, respectively.
[e]R_{free} is equal to R_{cryst} for a randomly selected 5% subset of reflections not used in the refinement (Brünger, 1992b).

The orientations of hRI and Ang with respect to each other are the same as in the pRI–RNase A complex: in both cases, about one-third of the ligand molecule sits inside the central cavity of the RI horseshoe with the remainder extending above it, and the enzymatic active site contacts the C-terminal portion of the inhibitor. Beyond these gross similarities, however, there are substantial differences in the modes of interaction in the two complexes, as will be detailed below.

The non-crystallographic dimer of hRI–Ang complexes is held together largely by a striking anti-parallel β-sheet constructed from the N-terminal 11 residues of each hRI molecule (Figure 2A; Table II). Residues 1–4 of each RI molecule protrude from their respective horseshoe rings and interact with residues 8–11 of the other RI molecule. To complete the sheet structure, N and O of each Ser6 hydrogen-bond to the corresponding O and N, respectively, of the other. In the resultant face-to-face arrangement of the two monomers, several residues outside the N-terminal region also form hydrogen bonds with the opposite molecule. Moreover, numerous water molecules (eight of them buried) are clustered in a cushion at the interface and participate in packing interactions. The RI monomer face involved in dimerization is opposite to that where Ang binds; hence Ang plays no direct role. The two interacting RI faces are not perfectly parallel, but are oriented at an angle of 15°, giving the dimer a 'jaw-like' appearance. In addition, the openings of the two horseshoes are staggered by ~80°.

In the crystal lattice, the dimer molecules which pack along the *x*-axis are held together mainly by two hydrogen bonds between hRI molecules: Glu441 OE2 to Arg187 NH2 (2.8 Å) and Gln77 OE1 to Gln423 NE2 (3.1 Å). In contrast, packing of dimers along the *y*-axis is stabilized by interactions between the Ang and RI molecules, most notably two hydrogen bonds from Gln77 NE2 of Ang (molecule 2) to Arg280 O and Pro310 O of hRI (molecule 1; 2.7 and 3.1 Å, respectively). Packing of dimers along the *z*-axis also involves both Ang and hRI molecules. The contribution of Ang is quite important, since in certain regions of the lattice the hRI molecules are some 20 Å apart.

General characteristics of the hRI–Ang interface

The contact surface is formed by 26 hRI residues on 13 discontinuous segments of the polypeptide chain (in 13 different repeat units), and 24 residues on seven segments of Ang (Table III, Figure 4). Twenty-five of the RI residues lie on β–α loops or β-strands (i.e. on the top face and inside the cavity of the horseshoe); the remaining one is at the beginning of an α-helix. The contacts on Ang are distributed over three of the protein's four helices, three of its five β-strands and four of its eight loops.

Formation of the hRI–Ang complex buries 2908 Å^2 of the accessible surface areas of the two proteins, about the same as the area buried in the pRI–RNase A complex, 2878 Å^2. [Areas were calculated with the program DSSP (Kabsch and Sander, 1983); the value for the latter complex is somewhat higher than that determined by Kobe and Deisenhofer (1995, 1996) with the program SURFACE (CCP4, 1994).] These areas are much larger than those reported for the barnase–barstar complex [~1600 Å^2

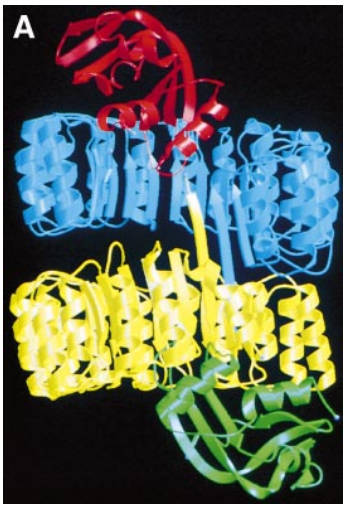

Fig. 2. (**A**) Overall view of the hRI–Ang dimer (perpendicular to the plane of the horseshoe), drawn with the program MOLSCRIPT (Kraulis, 1991). The hRI molecules are in cyan and yellow, and the Ang molecules are shown in red and green. (**B**) Stereo view of a C^{α} trace of the hRI–Ang complex superimposed on the pRI–RNase A complex (Kobe and Deisenhofer, 1995). The colour codes are: green, hRI; red, pRI; blue, Ang; and cyan, RNase A. Drawn with the program MOLSCRIPT (Kraulis, 1991). (C and D) Molecular surfaces of hRI (**C**) and pRI (**D**) drawn with the program GRASP (Nicholls and Honig, 1991). Surface complementarity at the interface in hRI–Ang and pRI–RNase complexes is colour coded based on calculations using the program SHAPE (Lawrence and Colman, 1993). Red, yellow and light blue colours correspond to S_c values of 1.0, 0.5 and 0.0 respectively. The horseshoe was rotated by ~20° from the standard orientation in order better to show the inner surface of the C-terminal half, where many of the contacts are. For identification of hRI residues in regions of high complementarity, compare (C) with Figure 4A.

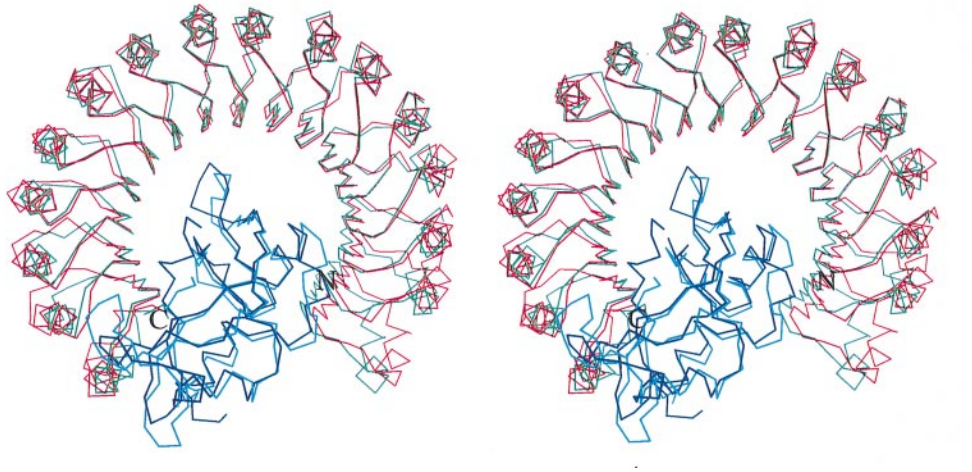

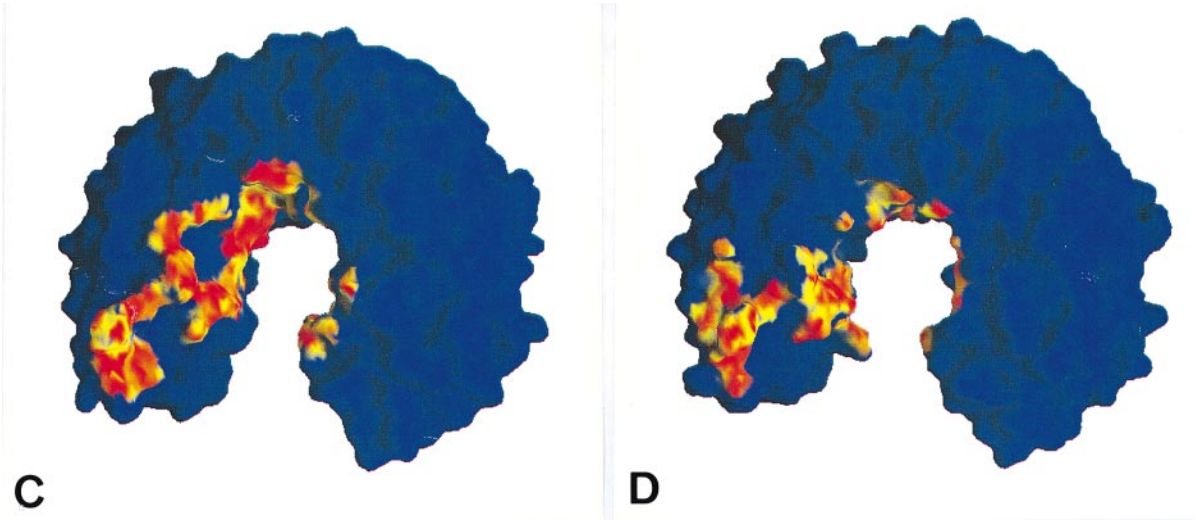

(Guillet *et al.*, 1993; Buckle *et al.*, 1994)], which has a dissociation constant (10^{-14} M; Hartley, 1993; Schreiber and Fersht, 1993) similar to that of the pRI–RNase A complex. Indeed, only a few complexes of heterologous proteins are known to have comparable or larger interface areas [cyclin A–CDK2 (Jeffrey *et al.*, 1995), thrombin–hirudin (Rydel *et al.*, 1991) and TEM-1 β-lactamase with its inhibitor BLIP (Strynadka *et al.*, 1996); for reviews, see Janin, 1995; Jones and Thornton, 1996]. The hRI–Ang interface is 55% non-polar, 22% uncharged polar and 23% charged. This distribution is similar to that in the pRI–RNase A complex (49% non-polar, 27% uncharged polar and 24% charged). However, the characters of the individual contact surfaces for enzyme and inhibitor in the two complexes are quite different: the buried surface on Ang is much more highly charged (30%) than that on

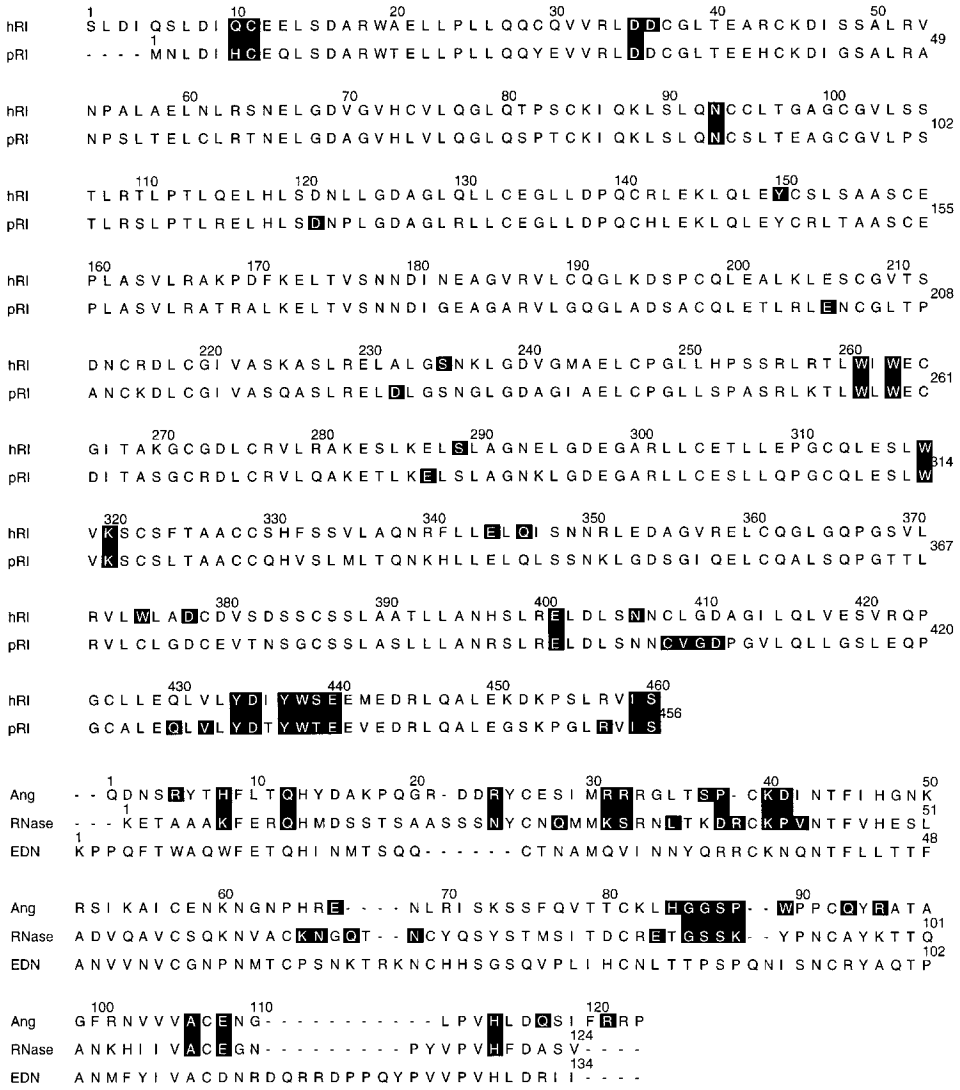

Fig. 3. Amino acid sequence alignment for (i) hRI (Lee *et al.*, 1988) and pRI (Hofsteenge *et al.*, 1988), and (ii) Ang (Strydom *et al.*, 1985), RNase A and EDN (Beintema *et al.*, 1988a). The contact residues are shown in boxes: for hRI and Ang as shown in Table III, for pRI and RNase as described by Kobe and Deisenhofer (1995, 1996). The figure was produced using ALSCRIPT (Barton, 1993). The secondary structure elements [based on the program DSSP (Kabsch and Sander, 1983)] contain the following residues: for hRI: β1 (1–10), βα1 (11–15), α1 (16–22), αβ1 (23–30), β2 (31–35), βα2 (36–43), α2 (44–52), αβ2 (53–58), β3 (59–61), βα3 (62–67), α3 (68–76), αβ3 (77–87), β4 (88–90), βα4 (91–100), α4 (101–110), αβ4 (111–115), β5 (116–118), βα5 (119–124), α5 (125–136), αβ5 (137–144), β6 (145–147), βα6 (148–157), α6 (158–167), αβ6 (168–172), β7 (173–175), βα7 (176–181), α7 (182–195), αβ7 (196–201), β8 (202–204), βα8 (205–213), α8 (214–224), αβ8 (225–229), β9 (230–232), βα9 (233–238), α9 (239–250), αβ9 (251–258), β10 (259–261), βα10 (262–268), α10 (269–279), αβ10 (280–286), β11 (287–289), βα11 (290–295), α11 (296–307), αβ11 (308–315), β12 (316–318), βα12 (319–328), α12 (329–338), αβ12 (339–343), β13 (344–346), βα13 (347–352), α13 (353–364), αβ13 (365–372), β14 (373–375), βα14 (376–385), α14 (386–395), αβ14 (396–400), β15 (401–403), βα15 (404–410), α15 (411–422), αβ15 (423–429), β16 (430–432), βα16 (433–439), α16 (440–452), αβ16 (453–456), β17 (457–458), βα17 (459–460); and for Ang: L1 (1–4), α1 (5–13), L2 (14–22), α2 (23–33), L3 (34–40), β1 (41–46), L4 (47–49), α3 (50–56), L5 (57–68), β2 (69–71), L6 (72–75), β3 (76–83), L7 (84–93), β4 (94–107), L8 (108–111), β5 (112–116), 3_{10} (117–123). Abbreviations: α, α-helix; β, β-sheet; L, αβ or βα loops.

RNase A (18%), and the reverse is true for the associated RI molecules (15% charged for hRI versus 29% for pRI).

The shape complementarity of the hRI–Ang interface was evaluated with the program SHAPE (Lawrence and Colman, 1993), which calculates a statistic, S_c, that ranges from 0 (no complementarity) to 1.0 (perfect complementarity). The overall S_c value obtained was 0.70, identical to that for the barnase–barstar complex (Buckle *et al.*, 1994) and considerably higher than that for the pRI–RNase A complex (0.58; Kobe and Deisenhofer, 1996). The solvent molecules do not appear to contribute to the complementarity at the interface. Examination of the local variation of S_c over the hRI surface (Figure 2C) reveals extended regions of particularly high complementarity in the C-terminal domain (the 434–440 loop) and the 11 to 12 o'clock portion of the horseshoe (tryptophans 261, 263 and 318), plus small pockets in the N-terminal domain (residues 10, 11, 35 and 36). The variation of S_c over the surface of pRI in its complex with RNase A (Figure 2D) is strikingly different: high complementarity is more heavily concentrated in the C-terminal region (segments 405–407 and 430–436, plus residue 456), with only a few, isolated spots scattered around the inside of the rest of the horseshoe.

Table II. Hydrogen bond interactions between the two hRI molecules (dimer interface) in the hRI–Ang complex

Molecule 1	Molecule 2	Distance (Å)
Ser1 N	Cys11 O	2.9
Leu2 N	Gln10 O	3.0
Leu2 O	Gln10 N	3.1
Ile4 N	Asp8 O	2.7
Ile4 O	Asp8 N	2.8
Ser6 N	Ser6 O	3.2
Ser6 O	Ser6 N	3.2
Asp8 N	Ile4 O	2.8
Asp8 O	Ile4 N	2.7
Gln10 N	Leu2 O	2.8
Gln10 O	Leu2 N	3.1
Cys11 O	Ser1 N	3.2
Arg142 NH2	Asp452 O	3.2
Arg142 NE	Asp452 O	3.2
Gln313 OE1	Gln313 NE2	2.9
Gln-313 NE2	Gln313 OE1	3.0
Glu429 OE2	Lys172 NZ	3.1
Asp452 O	Arg142 NH2	2.6

Table III. Contacts in the hRI–Ang complex structure

hRI residue	Ang residue(s)	No. of contacts
Gln10	Arg31	3
Cys11	Arg32	2
Asp35	Arg31	7
Asp36	Arg32	8
Asn93	Arg24	1
Tyr150	Gln93$^{(1)}$, Arg95$^{(1)}$	2
Ser235	His84	1
Trp261	Ser87	1
Trp263	Gly85$^{(7)}$, Gly86$^{(7)}$, His84$^{(4)}$	18
Ser289	Gly86	4
Trp318	Gly86$^{(1)}$,Ser87$^{(1)}$, Pro88$^{(5)}$, Trp89$^{(3)}$	10
Lys320	Asp41	1
Glu344	Trp89	6
Gln346	Pro88	1
Trp375	Pro88$^{(10)}$, Trp89$^{(3)}$	13
Asp378	Arg121	2
Glu401	Trp89	1
Asn406	Arg121	1
Tyr434	Lys40	7
Asp435	Lys40$^{(5)}$, Gln117$^{(4)}$	9
Tyr437	Glu67$^{(2)}$, Ala106$^{(2)}$, Glu108$^{(1)}$, His114$^{(4)}$	9
Trp438	Arg5	5
Ser439	Arg5$^{(1)}$, Glu108$^{(1)}$	2
Glu440	Arg5$^{(2)}$, Glu108$^{(1)}$	3
Ile459	Ser37$^{(1)}$, Pro38$^{(1)}$	2
Ser460	His8$^{(3)}$, Gln12$^{(2)}$	5

Contact distances are the maximum allowed values of C–C, 4.1 Å; C–N, 3.8 Å; C–O, 3.7 Å; O–O, 3.3 Å; O–N, 3.4 Å; and N–N, 3.4 Å Arg24, Glu67, Arg95 and Arg121 are partially disordered Ang residues in the hRI–Ang complex structure. Superscript numbers in parentheses represent the number of contacts made with the indicated Ang residue.

Details of the interactions at the interface

Ang and hRI form a total of 124 contacts (Table III and Figure 4C); 11 are potential hydrogen bonds (Table IV), and five of these are salt links. The vast majority of the interactions involve side-chain atoms. Only one main-chain element (from Trp438 of hRI) participates in a hydrogen bond, although main-chain atoms of Ang residues Arg32, Ser37, Gly85 and Gly86 and RI residues Ser439 and Glu440 form 22 of the van der Waals contacts. In addition to the direct interactions between the two proteins, there are 15 water-mediated hydrogen bonds (Table V).

The inhibitor makes extensive contacts with the ribonucleolytic active site of Ang. This site, like that of RNase A (Richards and Wyckoff, 1973), is usually described in terms of various subsites: these include a P_1 site where phosphodiester bond cleavage occurs, a B_1 site for the pyrimidine moiety of the nucleoside that donates its 3′ oxygen to the scissile bond, a B_2 site for the base of the nucleoside that donates its 5′ oxygen and a P_2 site for the 3′ phosphate of the B_2 nucleotide. Although no Ang–nucleotide complex structure has yet been determined, the residues that comprise these subsites have been inferred based on homology considerations and mutagenesis data. In the hRI–Ang complex, the ε-amino group of the catalytic P_1 residue Lys40 (Shapiro *et al.*, 1989) forms two hydrogen bonds with the carboxylate of Asp435 of RI (Figure 5A). In addition, the alkyl portion of the Lys40 side chain runs across the Tyr434 ring, making numerous van der Waals contacts. Another essential P_1 component, His114 (Shapiro and Vallee, 1989), forms several van der Waals contacts with Tyr437 (Figure 5B). Gln12 and His8 hydrogen-bond with Ser460 of hRI (Figure 5C); Gln12 is expected to be part of the P_1 site (Acharya *et al.*, 1994), whereas His8 is on the periphery of this site and may play an indirect role in catalysis (R.Shapiro, unpublished results). The P_2 site residue Arg5 (Shapiro and Vallee, 1992; Russo *et al.*, 1996) forms two hydrogen bonds with the carbonyl oxygen of Trp438 (Figure 5B) and van der Waals interactions with Ser439 and Glu440. Glu108, which lies within or near the B_2 site of Ang (Curran *et al.*, 1993; Acharya *et al.*, 1994), contacts Tyr437, Ser439 and Glu440 of RI; another possible B_2 component, Ala106, also interacts with Tyr437. Gln117, a residue that obstructs the B_1 site in the inactive conformation of native Ang (Acharya *et al.*, 1994; Russo *et al.*, 1994), makes van der Waals contacts with Asp435. Finally, Arg5 and Gln12 of Ang form water-mediated hydrogen bonds with Ile436 and Asp435, respectively, of hRI (Table V).

Several regions outside the active site of Ang are part of the interface with RI. The surface loop 84–89 makes a particularly large number of contacts (Figure 5D), involving four tryptophans (261, 263, 318 and 375) and five hydrophilic residues (Ser235, Ser289, Glu344, Gln346 and Glu401) on RI. This is one of the areas of highest complementarity between the two proteins (Figure 2C). The most striking feature here is the parallel packing of the indole ring of Trp263 against a planar portion of the Ang main chain that extends from N of Gly85 to C^{α} of Gly86. As indicated above, formation of this set of interactions entails a substantial change in the conformation of the Ang loop. The Trp318 indole group also runs parallel to the Ang main chain, in this case at Ser87 and Pro88, but for the most part is beyond van der Waals contact distance from the former residue. Trp318 and Trp375 effectively envelop Pro88 of Ang, making a total of 15 van der Waals contacts. Both of these RI residues also interact with Trp89 of Ang, as do Glu344 and Glu401. The Trp89–Glu344 interaction is the only direct hydrogen bond between the two proteins in this region. However, there are three water-mediated hydrogen bonds: Ang

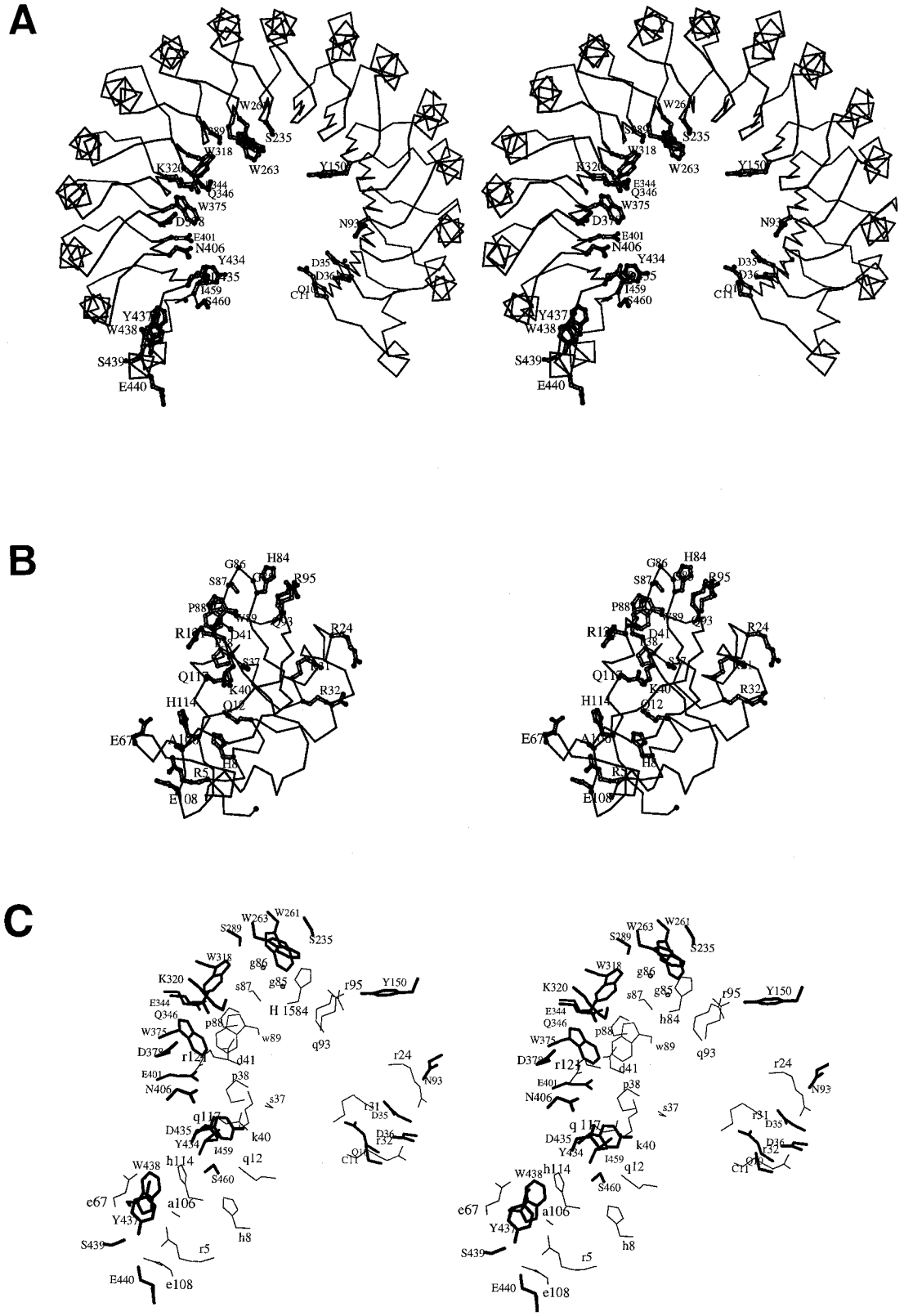

Fig. 4. Stereo views of hRI (**A**) and Ang (**B**) (C^{α} atoms plus side chains of contact residues), and hRI (thick lines, upper case letters) plus Ang (thin lines, lower case letters) together (contact residues only) (**C**) in the hRI–Ang complex.

Gly86 to both Glu206 and Trp263 of RI, and Ang Trp89 to Glu344 of RI (Table V).

Arg31 and Arg32, located at the end of α-helix 2 of Ang, engage in numerous interactions with the N-terminal region of RI. Arg31 is connected to Asp35 via two hydrogen bonds and several van der Waals interactions, and Arg32 forms a single hydrogen bond and multiple van der Waals contacts with Asp36 (Figure 5E). These

Table IV. Potential hydrogen bonds between hRI and Ang in the complex structure[a]

hRI	*B*-factor Å^2	Ang	*B*-factor Å^2	Distance D...A (Å)	D-H...A (°)
Trp438 O	39.8	Arg5 NH2	40.5	2.6	143
Trp438 O	39.8	Arg5 NH1	40.9	3.2	124
Ser460 OG	46.0	His8 NE2	40.4	2.8	136
Ser460 OG	46.0	Gln12 NE2	46.4	2.8	124
Asp35 OD2	39.5	Arg31 NH2	56.6	2.5	126
Asp35 OD1	38.2	Arg31 NH1	60.7	3.1	151
Asp36 OD1	43.3	Arg32 NH1	80.6	2.5	159
Asp435 OD1	37.3	Lys40 NZ	22.2	2.9	
Asp435 OD2	36.9	Lys40 NZ	22.2	3.0	
Glu344 OE1	48.1	Trp89 NE1	36.3	3.2	124
Tyr150 OH	71.2	Arg95 NH1	72.2	3.0	124

[a]All contacts shorter than 3.3 Å with D-H...A angle >120° are shown (D, hydrogen bond donor; A, hydrogen bond acceptor). Bond angles are not given for hydrogen bonds involving NZ atoms since the hydrogen position is ambiguous. Hydrogen bond parameters were calculated with the CCP4 program CONTACT (CCP4, 1994).

Table V. Water-mediated hydrogen bonds between hRI and Ang in the complex structure

Water	hRI residue	Distance (Å)	hAng residue	Distance (Å)	Solvent accessibility[a] (Å^2)	*B*-factor (Å^2)
1703	Asp435 OD1	2.6	Leu115 O	2.9	0.0	37.1
1704	Asp435 N	2.6	Gln12 OE1	3.4	1.8	24.6
1734	Glu206 OE2	3.3	Gly86 N	2.7	14.9	37.2
	Trp263 NE1	3.4				
1745	Asp36 OD2	3.4	Arg24 NH1	2.7	8.6	58.1
	Ser64 O	3.4				
1749	Asn178 OD1	3.4	Gln93 NE2	3.1	1.1	53.3
	Ser207 OG	2.8				
1825	Cys11 O	3.4	Arg32 NE	3.2	35.6	45.6
1846	Asp435 O	3.2	Gln117 N	2.8	7.3	38.0
1861	Asn406 OD1	2.8	Arg121 NH1	2.7	0.8	53.4
1862	Asp435 OD2	3.3	Asp41 N	3.3	2.5	39.9
	Asn406 OD1	2.8				
1865	Ile436 O	2.8	Arg5 NH2	3.2	6.4	46.8
1873	Glu344 OE2	2.9	Trp89 NE1	3.3	47.1	61.0

[a]Probe radius 1.4 Å [solvent accessibility calculated with the program XPLOR (Brünger, 1992a)].

arginines also contact Gln10 and Cys11, respectively, of RI.

A relatively small number of additional interactions are scattered around the inside of the RI horseshoe. Although one of these, between Arg95 of Ang and Tyr150 of RI, appears to satisfy the distance and angle requirements for a hydrogen bond, the high temperature factors associated with both components suggest that these residues may not in fact form such an interaction. Additional contacts involve the Ang–RI pairs Arg24–Asn93, Gln93–Tyr150, Asp41–Lys320, Arg121–Asp378, Ser37–Ile459 and Pro38–Ile459. In molecule 2 of the non-crystallographic dimer, the carboxylate of Ang Asp41 forms a 2.8 Å hydrogen bond with the ε-amino group of RI Lys320 that is not present in molecule 1.

Discussion

Correlation of structural data with the functional effects of mutagenesis and chemical modification

The interaction between hRI and Ang has been studied extensively by mutagenesis and chemical modification [see Table VI and Lee and Vallee (1989)]. The results of these investigations can now be interpreted in light of the structure of the complex. The most dramatic effect of any single-site mutation was the 1300-fold weakening of binding due to replacement of the Ang residue Lys40 by Gln (Lee and Vallee, 1989). The magnitude of this change suggested that Lys40 forms a strong hydrogen bond with hRI, and evidence obtained by mutagenesis of hRI later identified Asp435 as its likely partner on the inhibitor (Chen and Shapiro, 1997). Thus, substitution of Asp435 by Ala decreased binding affinity to almost the same extent as the Lys40 mutation, and the complex of K40Q-Ang with D435A-RI was found to dissociate at the same rate as the complex of K40Q with native RI (Chen and Shapiro, 1997). The crystal structure reveals that there are in fact two salt bridges between the ε-amino group of Lys40 and the carboxylate of Asp435 (Table IV, Figure 5A).

Mutation of the Ang residue Arg5 to Ala also increased the dissociation constant markedly, in this case by 50-fold (Shapiro and Vallee, 1992). This change can again be explained by the loss of interactions with the C-terminal region of RI: the crystal structure shows two hydrogen bonds between the guanidino group of Arg5 and the main-chain carbonyl oxygen of Trp438 on RI (Table IV, Figure 5B). More modest effects accompanied mutations of RI Ser460 and its hydrogen-bonding partners on Ang, His8 and Gln12 (Figure 5C) (Chen and Shapiro, 1997). The 8.5-fold increase in K_i for the des(460) RI derivative seems to be due largely to removal of the interaction of Ser460 with His8 rather than with Gln12, based on the relative changes produced by substituting these residues

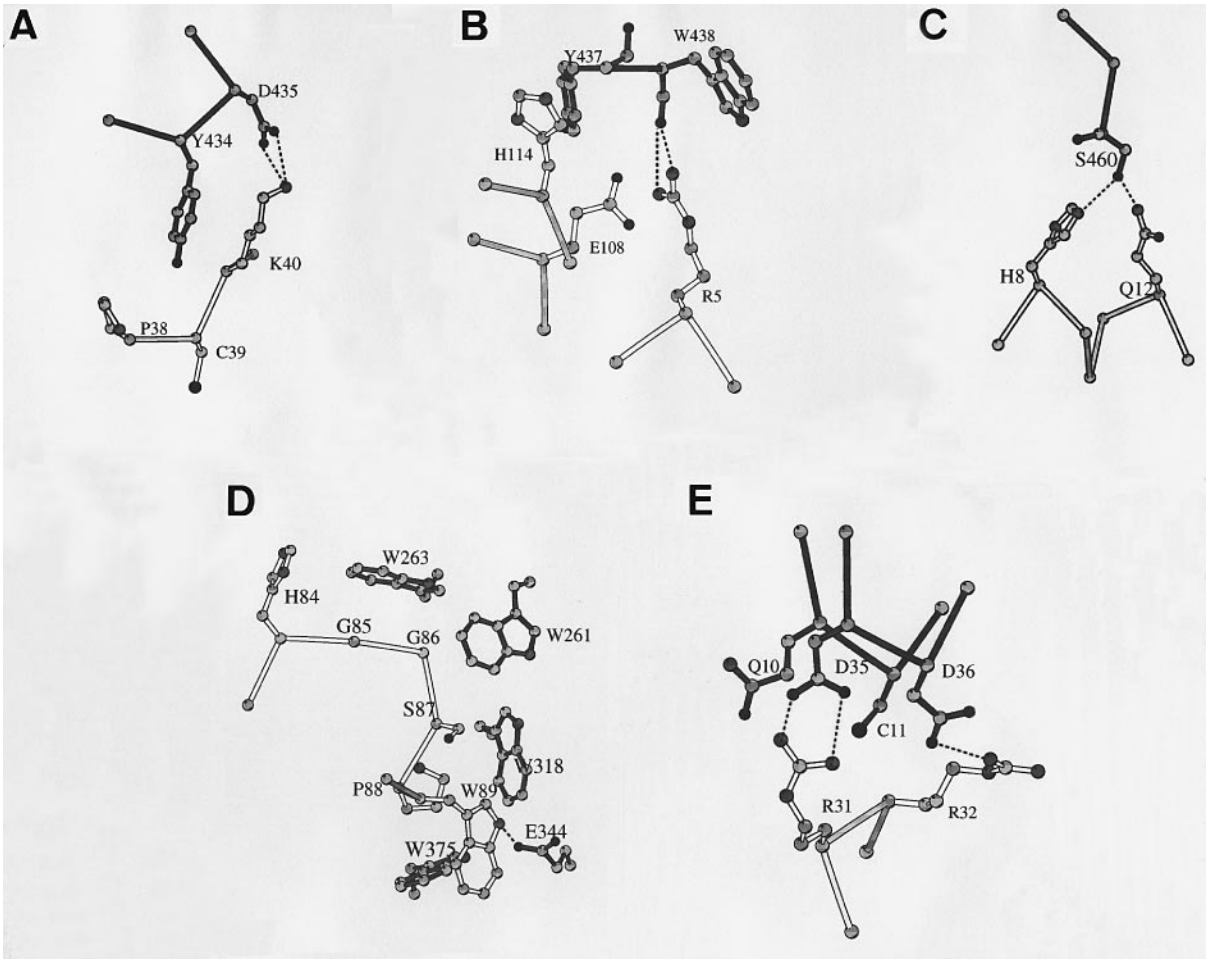

Fig. 5. (**A**–**E**) Detailed interactions at the hRI–Ang interface. hRI residues have filled bonds; Ang residues have empty bonds. Drawn with the program MOLSCRIPT (Kraulis, 1991).

individually by Ala (4.6- and 1.6-fold, respectively). There is no obvious explanation for the small magnitude of the effect of the Gln mutation. Replacements of His114 of Ang and Tyr437 of hRI resulted in small but significant decreases in binding affinity (Shapiro and Vallee, 1989; Chen and Shapiro, 1997). These residues make several van der Waals interactions in the crystal structure. The similarity of the consequences of the His114 and Tyr437 mutations suggests that the additional contacts of the tyrosine with Glu67, Ala106 and Glu108 of Ang (Table III) are weak. Indeed, Glu67 is partially disordered in the complex structure, and substitution of Glu108 by Ala has already been shown to have no adverse effect (Chen and Shapiro, 1997).

The hRI–Ang structure does not account for the kinetic properties of the RI mutant Y434A, which binds to Ang 246-fold less tightly than does native RI. Although Tyr434 makes seven van der Waals contacts with Lys40 of Ang (Figure 5A) and becomes almost completely buried upon complex formation (Figure 6), the effects of mutating Tyr434 and Lys40 are completely additive (Chen and Shapiro, 1997). This independence suggests that these two residues do not engage in energetically significant interactions with each other. It also indicates that the effect of the Tyr434 mutation on K_i does not stem from a perturbation of its important neighbour, Asp435.

Trp89 of Ang was proposed previously to be part of the interface with RI (Lee and Vallee, 1989; Lee *et al.*, 1989b) since (i) the marked increase in tryptophan fluorescence that accompanies formation of the hRI–Ang complex is abolished by oxidation of this residue, the only Trp in Ang, to oxindolalanine (which is not fluorescent); (ii) binding of RNase A (which contains no Trp) does not increase hRI fluorescence; (iii) Trp89 is highly accessible in native Ang but not in the hRI complex; and (iv) conversion of the Trp to oxindolalanine weakens hRI binding by 2.4-fold. The crystal structure shows that Trp89 indeed makes numerous contacts with RI (Table III, Figure 5D) and is largely buried (Figure 6). The energetic contribution of Trp89 cannot be quantitated from the effect of oxidation on binding because this modification enlarges, rather than removes, the side chain.

One additional Ang residue, Arg32, was proposed to contact RI: mutation of this amino acid to Ala decreases binding affinity by a factor of 4.6 (Shapiro and Vallee, 1992). In the crystal structure, Arg32 makes nine van der Waals contacts with Cys11 and Asp36 of hRI, and a hydrogen bond with the latter residue (Table IV, Figure 5E). However, the temperature factor for the Arg32 guanidino group is high, indicating that this hydrogen bond is weak at best. This is consistent with the relatively small change in K_i for this mutant.

Modifications of nine other Ang residues—His13, Arg31, Arg33, Lys50, Lys60, Arg66, Asn68, Arg70 and

Table VI. Effects of Ang and hRI modifications on binding[a]

Protein	Modification	$K_{i,mod}/K_{i,nat}$[b]	$\Delta\Delta G$[c] (kcal/mol)	Interface[d]
RI	Δ315–371[e]	76 000	6.6	yes
RI	Δ144–257[e]	2500	4.6	yes
Ang	Lys40→Gln	1300	4.2	yes
RI	Asp435→Ala	358	3.5	yes
RI	Tyr434→Ala	246	3.3	yes
Ang	Arg5→Ala	50	2.3	yes
RI	Δ460[e]	8.5	1.3	yes
Ang	His8→Ala	4.6	0.9	yes
Ang	Arg32→Ala	4.6	0.9	yes
RI	Tyr437→Ala	4.1	0.8	yes
Ang	His114→Ala	3.0	0.6	yes
Ang	Trp89→Oia[f]	2.4	0.5	yes
Ang	Arg33→Ala	1.7	0.3	no
Ang	Gln12→Ala	1.6	0.3	yes
Ang	Arg31→Ala	1.5	0.2	yes
Ang	Arg66→Ala	1.4	0.2	no
Ang	Asn68→Ala	1.2	0.2	no
Ang	Lys50→DNP-Lys[g]	0.9	–0.1	no
Ang	Lys60-DNP-Lys[g]	0.9	–0.1	no
Ang	Arg70→Ala	0.7	–0.2	no
Ang	His13→Ala	0.6	–0.3	no
Ang	Glu108→Ala	0.6	–0.3	yes

[a]References are given in the text.
[b]K_i for modified Ang or hRI divided by K_i for native proteins. Conditions are 0.1 M MES, 0.1 M NaCl, 1 mM EDTA, pH 6, 25°C.
[c]Difference in free energies of binding native and modified proteins, calculated from the equation $\Delta\Delta G = -RT \ln(K_{i,nat}/K_{i,mod})$. The ΔG value for the native hRI–Ang complex is –21.0 kcal/mol.
[d]Indicates whether the residue or region modified is part of the interface in the hRI–Ang crystal structure.
[e]Residues following the symbol 'Δ' have been deleted [des(460) RI].
[f]Oxindolalanine.
[g]Dinitrophenyllysine.

Glu108—had no significant effect on RI binding affinity. All but two of these residues, Arg31 (Shapiro and Vallee, 1992) and Glu108 (Chen and Shapiro, 1997), are now seen to lie outside the structural interface. Glu108 makes only a few van der Waals contacts with RI. In contrast, Arg31 appears to form two hydrogen bonds with Asp35 of RI, one of them only 2.5 Å in length (Table IV), and is buried in the complex (Figure 6). This residue, therefore, might have been expected to play a functional role. However, the relatively high temperature factors for NH1 and NH2 of Arg31 (Table IV) may imply that these atoms in fact do not engage in strong hydrogen bonds with Asp36. Alternatively, the Arg31 mutation might result in the formation of a new RI–Ang interaction or the strengthening of an existing one that compensates for the loss of these contacts.

In addition to the various singly modified derivatives of Ang and RI, two RI mutants that lack large segments of the protein have been kinetically characterized (Lee and Vallee, 1990). In one mutant, repeat units 6–9 (residues 144–257) were deleted; in the other, repeat units 12 and 13 (residues 315–371) were removed. These mutations decreased binding affinity by 2500- and 76 000-fold, respectively. The hRI–Ang complex structure reveals that the 144–257 deletion directly eliminates two contact residues, whereas the 315–371 deletion eliminates four. However, these mutations also have potentially important indirect effects due to the unusual structure of RI. Deletion of an internal repeat unit alters the relative positions of the contact residues on either side of it, thereby removing the interactions of one or the other of these sets of residues with Ang. In this case, the functional consequences of the deletion might be out of proportion to the importance of the residues lost. The deletion might also perturb the overall RI structure and/or introduce steric clashes between Ang and RI or between the newly juxtaposed repeats of RI. On the other hand, formation of favourable interactions between Ang and repositioned RI residues might compensate in part for the negative effects of the deletions. Therefore, the contributions of contact residues in the segments 144–257 and 315–371 cannot be deduced from the properties of these mutants.

Structural basis for tight binding of Ang to hRI

The RI–Ang contact surface is large and includes residues from nearly all repeat units of RI and several regions of Ang. Nonetheless, the combined structural and functional data discussed in the preceding sections indicate that a substantial fraction of the free energy of complex formation derives from contacts involving only a relatively small part of each molecule, the C-terminal segment of RI (434–460) and the P_1 and P_2 subsites of the Ang active centre (Figures 5A–C). These interactions seem to provide the major anchor for the attachment of the two molecules. The RI loop 434–440 makes a particularly strong contribution through hydrogen bonds involving the Asp435 carboxylate and the Trp438 main chain, van der Waals contacts of Tyr437 and interactions of Tyr434 that remain to be defined. If the changes in binding free energy that accompany the losses of these contacts (i.e. Ala mutations of hRI residues Tyr434, Asp435 and Tyr437 plus Arg5 of Ang) are additive, this single loop could potentially account for nearly half of the total (9.9 out of 21.0 kcal/mol). Ser460, which contributes another 1.3 kcal/mol, is located immediately adjacent to the loop.

The RI–Ang structure suggests that another part of the interface, containing four tryptophans of RI (261, 263, 318 and 375) and the 84–89 loop of Ang, is also functionally important (Figure 5D). This region has not yet been examined by mutagenesis. However, it seems likely to play a significant role based on (i) the high degree of complementarity between the hRI and Ang surfaces in this area (Figure 2C); (ii) the large number of intermolecular contacts it contains (53; 43% of the total) (Table III); (iii) the low-to-moderate temperature factors for the contact residues on both proteins; and (iv) the marked change in the structure of the Ang loop that accompanies complex formation. The packing of the RI residue Trp263 against the 85–86 segment of the polypeptide chain seems especially favourable. Beyond the C-terminal and Trp-rich regions of hRI, individual interactions of Asp36 and other scattered residues appear to provide small quantities of additional binding energy, mostly through van der Waals contacts.

The RI–Ang complex shares key features with other protein–protein complexes that have been investigated by both structural and functional approaches [e.g. the complex of human growth hormone with its receptor (de Vos *et al.*, 1992; Clackson and Wells, 1995), the barnase–barstar complex (Guillet *et al.*, 1993; Buckle *et al.*, 1994; Schreiber and Fersht, 1995), the pRI–RNase A complex (Kobe and Deisenhofer, 1995; Chen and Shapiro, 1997) and the

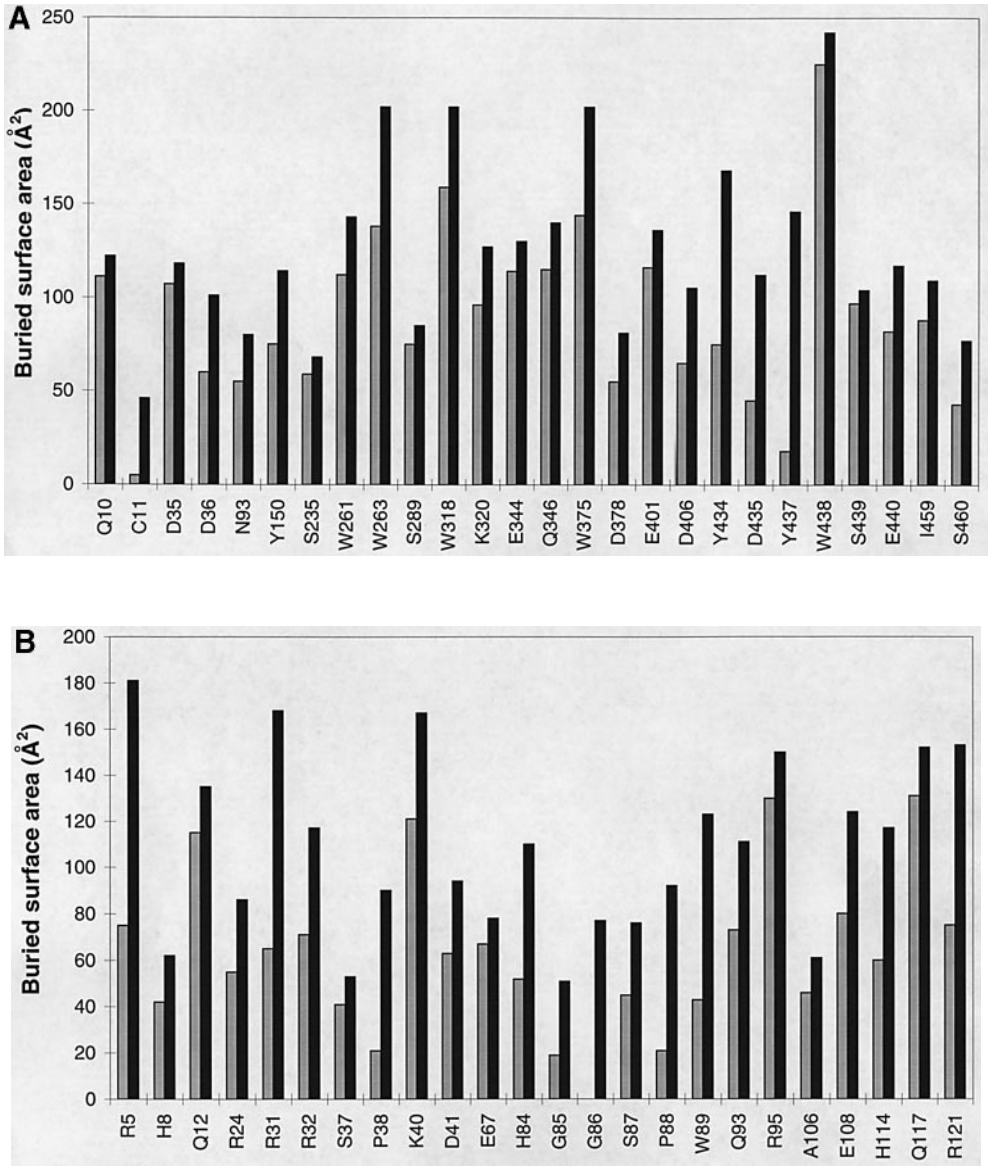

Fig. 6. Buried surface areas for each contact residue on hRI (**A**) and Ang (**B**) in the free proteins (stippled bars; calculated by separating hRI and Ang from the complex structure) and in the complex (solid bars). Accessible surface areas were calculated with the program XPLOR (Brünger, 1992a) and then subtracted from the theoretical maxima for a fully extended peptide chain Ala–X–Ala (dihedral angles all *trans*). The buried surface areas shown are for side-chain atoms, except in the cases of Trp438, Ser439 and Glu440 of hRI, plus Ser37, Gly85 and Gly86 of Ang, where the total contribution of the residue was used since main-chain atoms provide most or all of the contacts. Maximum accessibility values were taken from Richards and Wyckoff (1973), except for that of Trp (not given in this reference), which represents the total value of Chothia (1976) minus a typical main-chain contribution of 46 Å^2. These maxima are as follows: Gly (82); Ala (62); Pro (100); Ile (135); Ser (85 for side chain and 132 for total); Tyr (182); Asp/Asn (118); Glu/Gln (154 for side chain and 200 for total); His (145); Lys (170); Arg (211); Cys (48); Trp (209 for side chain and 255 for total).

complex between anti-lysozyme and its antibody (Fields *et al.*, 1995; Goldman *et al.*, 1997)]. In all of these, much of the structural interface is functionally inert and the existence of 'hot-spots', i.e. individual amino acids that make large energetic contributions (>3 kcal/mol), has been demonstrated. Thus far, the importance of specific contact residues, as revealed by mutagenesis, cannot be predicted reliably from an examination of the structure, even if this structure has been determined at high resolution as in the present case. In general, the correlation between the functional contribution of a residue and the degree to which it is buried in the complex is relatively poor (e.g. compare Figure 6 and Table VI). Moreover, contacts that apparently satisfy the distance and angle requirements for hydrogen bonds often have a minor role, if any (e.g. compare Tables IV and VI). However, the present analysis suggests that in some cases the temperature factors measured for contact residues may provide a useful criterion for judging the strength of the observed interactions. Indeed, consideration of these factors in the pRI–RNase A complex structure (Kobe and Deisenhofer, 1995, 1996; PDB code 1DFJ) indicates that some short contacts classified as salt links (e.g. Glu397 and Arg453 of pRI with Arg39 and Asp38, respectively, of RNase A) are nonetheless weak, in agreement with mutagenesis data (Chen and Shapiro, 1997).

Differences in the structural bases for recognition of Ang and RNase A by RI

In the crystal structure of the pRI–RNase A complex (Kobe and Deisenhofer, 1995, 1996), 24 RNase residues were found to be part of the contact surface. Comparison of the structures of RNase A and Ang (Acharya *et al.*, 1994) suggested that the interactions of most of these amino acids cannot be replicated in the RI–Ang complex and, therefore, that hRI recognizes the two ligands in largely different ways (Shapiro *et al.*, 1995). Subsequent support for this view came from mutagenesis of hRI, which showed that three major contact residues for RNase A on RI (Tyr434, Tyr437 and Ser460) are substantially less important for binding Ang (Chen and Shapiro, 1997). The RI–Ang crystal structure now reveals the details and extent of the differences in the binding modes.

Only nine contact residues on RNase A and Ang (out of 24 in each case) are identical or conservatively replaced in the primary structures (Figure 3). Seventeen of the residues that RI uses to bind RNase A and Ang (out of 28 and 26, respectively) are the same. The scope of the differences in the complexes is in fact even greater than these numbers indicate, because in many instances residues that seem to correspond in the Ang–RNase and hRI–pRI pairs do not engage in similar interactions. Trp438 in hRI hydrogen-bonds to Arg5 of Ang, whereas Trp434 in pRI only makes a van der Waals contact with Glu111 of RNase A. Tyr433 of pRI hydrogen-bonds with Asn71 and Glu111 of RNase A, but Tyr437 of hRI does not form any hydrogen bonds with Ang (hence the much smaller observed contribution of this residue to binding of Ang). Tyr434 of hRI contacts a single Ang residue (Lys40), in contrast with Tyr430 of pRI, which has extensive interactions with four RNase residues (Leu35, Arg39, Lys41 and Pro42). Lys320 of hRI contacts Asp41 of Ang, whereas Lys316 of pRI interacts with Glu86 of RNase A. Although Trp257 and Trp259 of pRI and Trp261 and Trp263 of hRI contact corresponding portions of RNase A (88–89) and Ang (85–86), the geometries of these interactions are quite distinct. Ser456 of pRI and Ser460 of hRI form apparently similar hydrogen bonds with Lys7 of RNase A and His8 of Ang, but mutagenesis reveals the interaction with RNase to be much stronger than that with Ang (see Neumann and Hofsteenge, 1993; Chen and Shapiro, 1997). These differences, and yet others, are reflected in the dissimilar surface complementarity profiles for the two complexes (Figure 2C and D).

One major difference between the RNase A and Ang complex structures is probably a crystallization artefact. In the hRI–Ang complex, which was crystallized with PEG as the precipitant, Asp435 of RI hydrogen-bonds to the P_1 site residue Lys40. This interaction is not present in the pRI–RNase complex, which was crystallized with ammonium sulfate, and the corresponding RNase residue (Lys41) instead binds a sulfate ion. Sulfate and other anions with affinity for the P_1 site are not present under the standard conditions used for kinetic characterization of RI complexes. Given the large, virtually identical decreases in the affinities of hRI for Ang and RNase A associated with mutation of Asp435 (Chen and Shapiro, 1997), it is highly likely that this residue forms similar hydrogen bonds with the catalytic lysine in both complexes.

Structural basis for broad recognition of pancreatic RNase superfamily proteins by RI

The various tight binding ligands of RI are all ribonucleolytic enzymes, and the crystal structures determined for these proteins thus far [RNase A (Richards and Wyckoff, 1973), Ang (Acharya *et al.*, 1994) and EDN (Mosimann *et al.*, 1996)] are all similar in terms of overall shape and 'α–β structure'. However, few amino acids are conserved throughout the family, and the average sequence identity between non-orthologous pairs is only ~30%. Particularly striking is the relatively poor conservation of the active site region, which places severe constraints on the mechanisms that can be used by an inhibitor to recognize all of these proteins. The pyrimidine-binding B_1 subsite is accessible in RNase A and EDN, but not in Ang, where it is obstructed by Gln117 (Acharya *et al.*, 1994; Russo *et al.*, 1994). It remains closed in the hRI complex. Two of the four residues considered to be part of the B_2 site in RNase A, Asn71 and Glu111, are maintained or conservatively replaced in the sequences of the other proteins, but their positions in the three-dimensional structures vary (Acharya *et al.*, 1994). The subsites extending farther away from the catalytic centre differ considerably. Lys66, a putative P_0 site residue in RNase A, is not retained in Ang, EDN and most other RNases. The P_2 site residues of RNase A (Lys7) and Ang (Arg5) do not correspond in terms of their positions in either the sequences or the structures; neither is present in EDN, which has Trp substitutions at both locations (the latter is C-glycosylated; Debur *et al.*, 1995).

Only the catalytic residues in the P_1 subsite (His13, Lys40 and His114 in Ang) are well conserved throughout the entire family. RI interacts with two of these residues in Ang, forming a strong hydrogen bond with Lys40 and weak contacts with His114. As discussed above, mutagenesis results indicate that it makes a functionally equivalent hydrogen bond with Lys41 in RNase A. Indeed, it seems likely that this interaction is replicated in all RI complexes and serves as a key common point of attachment. In the area around this contact, comprising the 434–440 loop and C-terminal serine of RI and the outer subsites of the ligand active site, additional interactions that are largely specific for the particular ligand may occur in all cases. The capacity of RI to form these contacts would reflect, on the one hand, the versatility and flexibility of the residues on this loop and, on the other hand, the 'stickiness' of ligand residues normally involved in binding RNA. Beyond the C-terminal region, residues lining the inside of the RI horseshoe probably make further ligand-specific contacts with amino acids well removed from the active site. The need to engage in such varied interactions may be a major reason for the large size and horseshoe shape of RI.

The results of modelling the RI–EDN complex are in good agreement with these proposals. The model was generated by superimposing the atomic coordinates for recombinant EDN (Mosimann *et al.*, 1996) onto those of Ang in the hRI–Ang complex and then performing energy minimization with the program XPLOR 3.1 (Brünger, 1992a). The resultant complex shows a reasonable fit between the two proteins and no obvious stereochemical impediments. However, only a few of the contacts in the model are similar to those in the Ang or RNase A

complexes. The active site lysine of EDN (Lys38), like that of RNase A, binds a sulfate ion (Mosimann *et al.*, 1996) and does not interact directly with Asp435 of RI. Again it seems likely that these residues would be able to form a good hydrogen bond if the sulfate were not present. Other interactions of the RI C-terminal region include multiple hydrogen bonds and van der Waals contacts of Gln447 and Ser460 with Lys1 of EDN, extensive contacts of Trp438, Glu443 and Ser460 with Trp7 (a possible P_2 site residue) and hydrogen bonds of Tyr434, Ile436 and Tyr437 with Gln34, His129 (P_1 site) and Asn70 (B_2 site), respectively (see Figure 3 for EDN amino acid sequence). Most of these are not present in the Ang or RNase A complexes. The model suggests that RI residues from several additional parts of the horseshoe may be involved in EDN recognition as well: Arg63 of RI hydrogen-bonds with Gln28, Ser94 and Asn95 of EDN; Asp121 hydrogen-bonds with Arg97; Trp263 contacts Thr86 and Thr87; Asp403 hydrogen-bonds with Arg36; and Asp411 hydrogen-bonds with Arg68. Again, virtually all of these interactions would be unique if they exist in the actual complex.

The effectiveness of RI against multiple RNase superfamily proteins, coupled with the diverse modes of recognition RI appears to use in achieving this, implies that it has evolved to inhibit all of these molecules. RI is present in the cytosol of all cells examined thus far, and, given the demonstrated cytotoxicity of RNases (including Ang) in general (Saxena *et al.*, 1991), it is reasonable to suppose that part of its function is to protect cells from any of these proteins that inadvertently enter this compartment (Beintema *et al.*, 1988b). Under some circumstances, RI may also act in the extracellular space, where it may participate in the regulation of Ang and other RNase family members such as the neurotoxins EDN and eosinophil cationic protein (Gleich *et al.*, 1986).

Prospects for development of small Ang antagonists that mimic RI

Several inhibitors of Ang have been demonstrated to have antitumour activity: anti-Ang monoclonal antibodies and the Ang-binding protein actin markedly affect the establishment and growth of human tumours in athymic mice (Olson *et al.*, 1994, 1995), and hRI interferes with the growth of syngeneic murine mammary tumours (Polakowski *et al.*, 1993). However, these agents are likely to have limited therapeutic utility in humans because of their large size and expense (all), immunogenicity (the antibodies), lack of specificity (actin and RI) and lability (RI). No small inhibitors of Ang with more suitable characteristics have been identified thus far. It is therefore of considerable interest to examine the implications of the present structural and functional information on the RI–Ang complex for the development of small RI mimics.

Three characteristics of the RI–Ang complex suggest that it may be feasible to obtain such an inhibitor. First, the complex is extraordinarily tight: its K_i value of 5×10^{-16} M is 6–7 orders of magnitude lower than would be required for *in vivo* effectiveness. Thus an RI derivative need not be capable of forming all of the energetically important interactions of the parent molecule. Second, a significant portion of the energy for binding Ang appears to be contributed by a single, relatively small domain of RI. The fit of this region to Ang could potentially be optimized further since it is no longer constrained by a need to interact with other RNase superfamily members. Third, although this domain of RI probably plays a critical role in binding all RI ligands, it seems to form many unique contacts with each of them. Thus the prospects for achieving a significant degree of specificity for Ang are favourable. Progress toward these ends will be facilitated by further dissection of the functional roles of individual contact residues on RI and Ang, now in progress, and by structural analyses of complexes of Ang and RI derivatives.

Materials and methods

Preparation, crystallization and data collection for the hRI–Ang complex

Natural hRI was obtained from the Promega Corporation (Madison, WI) or was purified from placenta (Blackburn, 1979). It was dialysed extensively against 20 mM HEPES, 20 mM DTT, pH 7.5 at 4°C and then concentrated by ultrafiltration. <Glu-1 human Ang was obtained from a recombinant system in *Escherichia coli* (Shapiro *et al.*, 1988) and dissolved in water. Protein concentrations were determined by amino acid analysis.

The hRI–Ang complex was formed by mixing 144 µl of 15.6 mg/ml inhibitor with 150 µl of 5.0 mg/ml Ang (i.e. in a molar ratio of 1:1.2) plus 15 µl of 0.2 M DTT and 6.3 µl of glycerol. This solution was stored under nitrogen at 4°C overnight before setting up crystallizations. Crystals were grown at 16°C by the vapour diffusion hanging drop method. Drops consisted of 2 µl of the complex mixed with an equal volume of reservoir solution containing 10% PEG 4000, 20 mM sodium citrate (pH 4.2), 0.1 M ammonium sulfate and 25 mM DTT. Although some of the protein precipitated immediately, small crystals appeared in the drops after 3–4 days, and continued to grow for about a week.

Two datasets were collected at room temperature. First, a low resolution dataset was collected at 2.8 Å resolution (in-house data) on a MAR Research image plate system (30 cm diameter) mounted on a Enraf–Nonius rotating anode X-ray generator using CuK_α radiation. The high resolution dataset (at 2.0 Å) was collected on station PX 9.6 (λ = 0.87 Å) of the Synchrotron Radiation Source, Daresbury, UK, using a 30 cm diameter MAR Research image plate system at room temperature. Indexing, scaling and merging of the data were performed using the programs DENZO (Otwinowski, 1993) and SCALA (CCP4, 1994).

Structure determination

The in-house data were used for structure determination and the merged high resolution dataset was used in the final refinement of the structure (details are presented in Table I). The determination of the hRI–Ang complex structure was performed by molecular replacement using the program AMoRe (Navaza, 1994). A polyalanine model of free pRI (all 456 residues) [PDB entry code 1BNH (Kobe and Deisenhofer, 1993)] was used as a search probe. However, this model failed to give an unambiguous solution. This problem was overcome by including both main-chain and side-chain atoms for the entire model (with replacement of non-conserved residues by alanines) and by excluding the first 20 amino acid residues at the N-terminus. Clear solutions were found in the cross-rotation and translation functions for both hRI molecules which, when combined, resulted in an *R*-factor of 47.9% after rigid body refinement in AMoRe, for data between 8 and 3.5 Å. Surprisingly, the two Ang molecules could not be located by molecular replacement [the search was based on the refined structure of free Ang at 2.0 Å (D.D.Leonidas, S.C.Allen and K.R.Acharya, unpublished results)]. Instead their positions in the complex were located by examination of the electron density map (calculated using the phase information from the two hRI molecules) in combination with mutagenesis results (Chen and Shapiro, 1997), which indicated definite contact points between hRI and Ang molecules.

Refinement

Refinement was first carried out using the in-house data at 2.8 Å resolution with standard protocols in program XPLOR (Brünger, 1992a), maintaining tight non-crystallographic symmetry restraints between the two molecules, and was alternated with manual rebuilding in the interactive graphics program O (Jones *et al.*, 1991). The progress of

the refinement was monitored throughout the process using both the conventional and free *R*-factors (R_{cryst} and R_{free}, Brünger, 1992b). A simulated annealing for the two hRI molecules alone resulted in an R_{free} of 41.5% (starting value 42.2%) and an R_{cryst} of 32.2% (starting value 38.3%). After the inclusion of the two Ang molecules, R_{free} dropped to 35.7% and R_{cryst} to 27.3%. Average electron density maps were calculated using the density modification program (DM) as implemented in the CCP4 package (CCP4, 1994). To minimize model bias in the calculated electron density maps, the program SIGMAA (Read, 1986) was used to obtain weighted map coefficients for use in the calculation of difference Fourier syntheses of the type $|F_{obs}|-|F_{calc}|$ and $2|F_{obs}|-|F_{calc}|$. The new high resolution dataset (merged with the in-house dataset) at 2.0 Å was used as the master set at this stage. Further refinement (in 0.1 Å resolution steps), model building, individual temperature factor (*B*-factor) refinement and, finally, bulk solvent correction with XPLOR (using all data, 72 308 reflections, 20–2 Å) resulted in a final model with R_{cryst} of 19.3% and last recorded R_{free} of 28.6% (3585 reflections). During the final stages of the refinement, ordered water molecules (with *B*-factors <65 Å^2) were added to the model. In hRI, the side chains of residues 22, 30, 123, 168, 194, 216, 237, 270, 294, 358, 383, 422, 451 and 452 have poor electron density and were modelled as alanines. For Ang, the three N-terminal residues have high temperature factors, and the side chains of the last three C-terminal residues display varying degrees of disorder in the two molecules. Apart from these residues, Arg24, Arg51, Arg70 plus the segment 58–68 in molecule 1, and Gln19, Arg24, Arg51 plus the segment 58–66 in molecule 2 are disordered, with *B*-factors >90 Å^2. Analysis of the Ramachandran (ϕ–ψ) plot [using the program PROCHECK (Laskowski *et al.*, 1993)] showed that all residues (except Ser15 in both molecules, and Ser4, Glu58 and Gln353 in RI molecule 2) lie in energetically allowed regions.

The atomic coordinates of the hRI–Ang complex will be deposited in the Brookhaven Protein Data Bank.

Acknowledgements

We thank the staff at the Synchrotron Radiation Source, Daresbury, UK, for their support during X-ray data collection. We also thank Drs B.L.Vallee and J.F.Riordan for advice and support, Dr C.-Z.Chen for kinetic measurements, Dr V.Nobile for hRI, Drs J.Deisenhofer and B.Kobe for the pRI–RNase A complex coordinates, Drs M.N.G.James and S.Mosimann for EDN atomic coordinates, and Dr M.Lawrence for the surface complementarity program. This work was funded by grants from the Medical Research Council (UK), the Cancer Research Campaign (UK) (K.R.A.), the Wellcome Trust (UK), (Grant 044107/Z/95/Z to K.R.A. and R.S., Grant 043614/Z/95/Z to K.R.A.), National Institutes of Health (Grant HL52096 to R.S.) and the Endowment for Research in Human Biology, Inc., Boston (R.S.).

References

Acharya,K.R., Shapiro,R., Allen,S.C., Riordan,J.F. and Vallee,B.L. (1994) Crystal structure of human angiogenin reveals the structural basis for its functional divergence from ribonuclease. *Proc. Natl Acad. Sci. USA*, **91**, 2915–2919.

Barton,G.J. (1993) ALSCRIPT: a tool to format multiple sequence alignments. *Protein Eng.*, **6**, 37–40.

Beintema,J.J., Hofsteenge,J., Iwama,M., Morita,T., Ohgi,K., Irie,M., Sugiyama,R.H., Schieven,G.L., Dekker,C.A. and Gleitz,D.G. (1988a) Amino acid sequence of the non-secretory ribonuclease of human urine. *Biochemistry*, **27**, 4530–4538.

Beintema,J.J., Schuller,C., Irie,M. and Carsana,A. (1988b) Molecular evolution of the ribonuclease superfamily. *Prog. Biophys. Mol. Biol.*, **51**, 165–192.

Bicknell,R. and Vallee,B.L. (1988) Angiogenin activates endothelial cell phospholipase C. *Proc. Natl Acad. Sci. USA*, **85**, 5961–5965.

Bicknell,R. and Vallee,B.L. (1989) Angiogenin stimulates endothelial cell prostacyclin secretion by activation of phospholipase A_2. *Proc. Natl Acad. Sci. USA*, **86**, 1573–1577.

Blackburn,P. (1979) Ribonuclease inhibitor from human placenta: rapid purification and assay. *J. Biol. Chem.*, **254**, 12484–12487.

Blackburn,P., Wilson,G. and Moore,S. (1977) Ribonuclease inhibitor from human placenta. *J. Biol. Chem.*, **252**, 5904–5910.

Boix,E., Wu,Y., Vasandani,V.M., Saxena,S.K., Ardelt,W., Ladner,J. and Youle,R.J. (1996) Role of the N-terminus in RNase A homologs—differences in catalytic activity, ribonuclease inhibitor interaction and cytotoxicity. *J. Mol. Biol.*, **257**, 992–1007.

Brünger,A.T. (1992a) *X-PLOR manual: Version 3.1. A System for Crystallography and NMR*. Yale University Press, New Haven, CT.

Brünger,A.T. (1992b) Free *R* value: a novel statistical quantity for assessing the accuracy of crystal structures. *Nature*, **355**, 472–474.

Buckle,A.M., Schreiber,G. and Fersht,A.R. (1994) Protein–protein recognition: crystal structure analysis of a barnase–barstar complex at 2.0Å resolution. *Biochemistry*, **33**, 8878–8889.

Chen,C.-Z. and Shapiro,R. (1997) Site-specific mutagenesis reveals differences in the structural bases for tight binding of ribonuclease inhibitor to angiogenin and ribonuclease A. *Proc. Natl Acad. Sci. USA*, **94**, 1761–1766.

Chothia,C. (1976) The nature of the accessible and buried surfaces in proteins. *J. Mol. Biol.*, **105**, 1–12.

Clackson,T. and Wells,J.A. (1995) A hot spot of binding energy in a hormone–receptor interface. *Science*, **267**, 383–386.

Collaborative Computational Project, Number 4 (1994) The CCP4 suite: programs for protein crystallography. *Acta Crystallogr.*, **D50**, 760–763.

Curran,T.P., Shapiro,R. and Riordan,J.F. (1993) Alteration of the enzymatic specificity of human angiogenin by site-directed mutagenesis. *Biochemistry*, **32**, 2307–2313.

Debur,T., Vliegenthart,J.F.G., Loffler,A and Hofsteenge,J. (1995) The hexpyranosyl residue that is C-glycosidically linked to the side chain of tryptophan-7 in human ribonuclease U_S is alpha-marmopyranose. *Biochemistry*, **34**, 11785–11789.

de Vos,A.M., Ultsch,M. and Kossiakoff,A.A. (1992) Human growth hormone and extracellular domain of its receptor—crystal structure of the complex. *Science*, **255**, 306–312.

Fett,J.W., Strydom,D.J., Lobb.,R.R., Alderman,E.M., Bethune,J.L., Riordan,J.F. and Vallee,B.L. (1985) Isolation and characterization of angiogenin, an angiogenic protein from human carcinoma cells. *Biochemistry*, **24**, 5480–5486.

Fields,B.A., Goldbaum,F.A., Ysern,X., Poljak,R.J. and Mariuzza,R.A. (1995) Molecular basis of antigen mimicry by an anti-idiotope. *Nature*, **374**, 739–742.

Gleich,G.J., Loegering,D.A., Bell,M.P., Checkel,J.L., Ackerman,S.J. and McKean,D.J. (1986) Biochemical and functional similarities between human eosinophil derived neurotoxin and eosinophil cationic protein—homology with ribonuclease. *Proc. Natl Acad. Sci. USA*, **83**, 3146–3150.

Goldman,E.R., Dall'Acqua,W., Braden,B.C. and Mariuzza,R.A. (1997) Analysis of binding interactions in an idiotope–antiidiotope protein–protein complex by double mutant cycles. *Biochemistry*, **36**, 49–56.

Guillet,V., Lapthorn,A., Hartley,R.W. and Mauguen,Y. (1993) Recognition between bacterial ribonuclease, barnase, and its natural inhibitor, barstar. *Structure*, **1**, 165–177.

Hallahan,T.W., Shapiro,R. and Vallee,B.L. (1991) Dual site model for the organogenic activity of angiogenin. *Proc. Natl Acad. Sci. USA*, **88**, 2222–2226.

Hartley,R.W. (1993) Directed mutagenesis of barnase–barstar recognition. *Biochemistry*, **32**, 5978–5984.

Hofsteenge,J. (1997) Ribonuclease inhibition. In D'Alessio,G. and Riordan,J.F. (eds), *Ribonucleases, Structures and Functions*. Academic Press, New York, pp. 621–658.

Hofsteenge,J., Kieffer,B., Matthies,R., Hemmings,B. and Stone,S.R. (1988) Amino acid sequence of the ribonuclease inhibitor from porcine liver reveals the presence of leucine-rich repeats. *Biochemistry*, **27**, 8537–8544.

Howlin,B., Moss,D.S. and Harris,G.W. (1989) Segmented anisotropic refinement of bovine pancreatic ribonuclease A by the application of rigid body TLS model. *Acta Crystallogr.*, **A45**, 851–861.

Hu,G.-F., Riordan.J.F. and Vallee,B.L. (1994) Angiogenin promotes invasiveness of cultured endothelial cells by stimulation of cell-associated proteolytic activities. *Proc. Natl Acad. Sci. USA*, **81**, 12096–12100.

Hu,G.-F., Riordan.J.F. and Vallee,B.L. (1997) A putative angiogenin receptor in angiogenin-responsive human endothelial cells. *Proc. Natl Acad. Sci. USA*, **94**, 2204–2209.

Janin,J. (1995) Elusive affinities. *Proteins: Struct. Funct. Genet.*, **21**, 30–39.

Janin,J. and Chothia,C. (1990) The structures of protein–protein recognition sites. *J. Biol Chem.*, **265**, 16027–16030.

Jeffrey,P.D., Russo,A.A., Polyak,K., Gibbs,E., Hurwitz,J., Massague,J. and Pavletich,N.P. (1995) Mechanism of CDK activation revealed by the structure of a cyclin A–CDK2 complex. *Nature*, **376**, 313–320.

Jimi,D.-i., Ito,K.-i., Kohno,K., Ono,M., Kuwano,M., Itagaki,Y. and Ishikawa,H. (1995) Modulation of bovine angiogenin of tubular morphogenesis and expression of plasminogen activator in bovine endothelial cells. *Biochem. Biophys. Res. Commun*., **211**, 476–483.

Jones,S. and Thornton,M. (1996) Principles of protein–protein interactions. *Proc. Natl Acad. Sci. USA*, **93**, 13–20.

Jones,T.A., Zou,J.Y., Cowan,S.W. and Kjeldgaard,M. (1991) Improved methods for building protein models in electron density maps and the location of errors in these models. *Acta Crystallogr.*, **A47**, 110–119.

Kabsch,W. and Sander,C. (1983) Dictionary of protein secondary structure: pattern recognition of hydrogen-bonded and geometrical features. *Biopolymers*, **22**, 2577–2637.

Kraulis,P.J. (1991) MOLSCRIPT—a program to produce both detailed and schematic plots of protein structures. *J. Appl. Crystallogr.*, **24**, 946–950.

Kobe,B. and Deisenhofer,J. (1993) Crystal structure of porcine ribonuclease inhibitor, a protein with leucine-rich repeats. *Nature*, **366**, 751–756.

Kobe,B. and Deisenhofer,J. (1995) A structural basis of the interactions between leucine-rich repeats and protein ligands. *Nature*, **374**, 183–186.

Kobe,B. and Deisenhofer,J. (1996) Mechanism of ribonuclease inhibition by ribonuclease inhibitor protein based on the crystal structure of its complex with ribonuclease A. *J. Mol. Biol*., **264**, 1028–1043.

Laskowski,R.A., MacArthur,M.W., Moss,D.S. and Thornton,J.M. (1993) PROCHECK: a program to check stereochemical quality of protein structures. *J. Appl. Crystallogr.*, **26**, 283–291.

Lawrence,M.C. and Colman,P.M. (1993) Shape complementarity at protein–protein interfaces. *J. Mol. Biol*., **234**, 946–950.

Lee,F.S. and Vallee,B.L. (1989) Binding of placental ribonuclease inhibitor to the active site of angiogenin. *Biochemistry*, **28**, 3556–3561.

Lee,F.S. and Vallee,B.L. (1990) Kinetic characterization of two active mutants of placental ribonuclease inhibitor that lack internal repeats. *Biochemistry*, **29**, 6633–6638.

Lee,F.S. and Vallee,B.L. (1993) Structure and action of mammalian ribonuclease (angiogenin) inhibitor. *Prog. Nucleic Acid Res*., **44**, 1–30.

Lee,F.S., Fox,E.A., Zhou,H.-M., Strydom,D.J. and Vallee,B.L. (1988) Primary structure of human placental ribonuclease inhibitor. *Biochemistry*, **27**, 8545–8553.

Lee,F.S., Shapiro,R. and Vallee,B.L. (1989a) Tight-binding inhibiton of angiogenin and ribonuclease A by placental ribonuclease inhibitor. *Biochemistry*, **28**, 225–230.

Lee,F.S., Auld,D.S. and Vallee,B.L. (1989b) Tryptophan fluorescence as a probe of placental ribonuclease inhibitor binding to angiogenin. *Biochemistry*, **28**, 219–224.

Moroianu,J. and Riordan,J.F. (1994) Nuclear translocation of angiogenin in proliferating endothelial cells is essential to its angiogenic activity. *Proc. Natl Acad. Sci. USA*, **91**, 1677–1681.

Mosimann,S.C., Newton,D.L., Youle,R.J. and James,M.N.G. (1996) X-ray crystallographic structure of recombinant eosinophil-derived neurotoxin at 1.83Å resolution. *J. Mol. Biol*., **260**, 540–552.

Navaza,J. (1994) AMoRe: an automated package for molecular replacement. *Acta Crystallogr.*, **A50**, 157–163.

Neumann,U. and Hofsteenge,J. (1994) Interaction of semisynthetic variants of RNase A with ribonuclease inhibitor. *Protein Sci*., **3**, 248–256.

Nicholls,A. and Honig,B. (1991) A rapid finite difference algorithm, utilising successive over relaxation to solve the Poisson–Boltzmann equation. *J. Comput. Chem*., **12**, 435–445.

Olson,K.A. and Fett,J.W. (1996) Prostatic carcinoma therapy with angiogenin antagonists. *Proc. Am. Assoc. Cancer Res.*, **37**, 57.

Olson,K.A., French,T.C., Vallee,B.L. and Fett,J.W. (1994) A monoclonal antibody to human angiogenin suppresses tumor growth in athymic mice. *Cancer Res*., **54**, 4576–4579.

Olson,K.A., Fett,J.W., French,T.C., Key,M.E. and Vallee,B.L. (1995) Angiogenin antagonists prevent tumor growth *in vivo*. *Proc. Natl Acad. Sci. USA*, **92**, 442–446.

Otwinowski,Z., (1993) Oscillation data reduction program. In Sawyer,L., Isaacs,N. and Bailey,S. (eds), *Data Collection and Processing*, *Proceedings of CCP4 Study Weekend*. SERC Daresbury Laboratory, Warrington, UK, pp. 56–62.

Polakowski,I.J., Lewis,M.K., Muthukkaruppan,V., Erdman,B., Kubai,L. and Auerbach,R. (1993) A ribonuclease inhibitor expresses anti-angiogenic properties and leads to reduced tumor growth in mice. *Am. J. Pathol*., **143**, 507–517.

Read,R.J. (1986) Improved Fourier coefficients for maps using phases from partial structures with errors. *Acta Crystallogr.*, **A42**, 140–149.

Richards,F.M. and Wyckoff,H.W. (1973) Ribonuclease S. Phillips,D.C. and Richards,F.M. (eds), *The Atlas of Molecular Structures in Biology. Volume I.* Clarendon Press, Oxford.

Russo,N., Shapiro,R., Acharya,K.R., Riordan,J.F. and Vallee,B.L. (1994) The role of glutamine-117 in the ribonucleolytic activity of human angiogenin. *Proc. Natl Acad. Sci. USA*, **91**, 2920–2924.

Russo,N., Acharya,K.R., Vallee,B.L. and Shapiro,R. (1996) A combined kinetic and modeling study of the catalytic center subsites of human angiogenin. *Proc. Natl Acad. Sci. USA*, **93**, 804–808.

Rydel,T.J., Tulinsky,A., Bode,W. and Huber,R. (1991) Refined structure of the hirudin–thrombin complex. *J. Mol. Biol*., **221**, 583–601.

Saxena,S.K., Rybak,S.M., Winkler,G., Meads,H.M., McGray,P., Youle,R.J. and Ackerman,E.J. (1991) Comparison of ribonucleases and toxins upon injection into *Xenopus* oocytes. *J. Biol. Chem*., **266**, 21208–21214.

Schreiber,G. and Fersht,A.R. (1993) Interaction of barnase with its polypeptide inhibitor barstar studies by protein engineering. *Biochemistry*, **32**, 5145–5150.

Schreiber,G. and Fersht,A.R. (1995) Energetics of protein–protein interactions: analysis of the barnase–barstar interface by single mutations and double mutant cycles. *J. Mol. Biol*., **248**, 478–486.

Shapiro,R. and Vallee,B.L. (1987) Human placental ribonuclease inhibitor abolishes both angiogenic and ribonucleolytic activities of angiogenin. *Proc. Natl Acad. Sci. USA*, **84**, 2238–2241.

Shapiro,R. and Vallee,B.L. (1989) Site-directed mutagenesis of histidine-13 and histidine-114 of human angiogenin. Alanine derivatives inhibit angiogenin-induced angiogenesis. *Biochemistry*, **28**, 7401–7408.

Shapiro,R. and Vallee,B.L. (1991) Interaction of human placental ribonuclease with placental ribonuclease inhibitor. *Biochemistry*, **30**, 2246–2255.

Shapiro,R. and Vallee,B.L. (1992) Identification of functional arginines in human angiogenin by site-directed mutagenesis. *Biochemistry*, **31**, 12477–12485.

Shapiro,R., Fett,J.W., Strydom,D.J. and Vallee,B.L. (1986) Isolation and characterization of a human-colon carcinoma secreted enzyme with ribonuclease-like activity. *Biochemistry*, **25**, 7255–7264.

Shapiro,R., Weremowicz,S., Riordan,J.F. and Vallee,B.L. (1987) Ribonucleolytic activity of angiogenin—essential histidine, lysine and arginine residues. *Proc. Natl Acad. Sci. USA*, **84**, 8783–8787.

Shapiro,R., Harper,J.W., Fox,E.A., Jansen,H.-W., Hein,F. and Uhlmann,E. (1988) Expression of Met-(–1) angiogenin in *Escherichia coli*—conversion to the authentic <Glu-1 protein. *Anal. Biochem.*, **175**, 450–461.

Shapiro,R., Fox,E.A. and Riordan,J.F. (1989) Role of lysines and human angiogenin—chemical modification and site-directed mutagenesis. *Biochemistry*, **28**, 1726–1732.

Shapiro,R., Riordan,J.F. and Vallee,B.L. (1995) LRRning the RIte of springs. *Nature Struct. Biol*., **2**, 350–354.

Soncin,F. (1992) Angiogenin supports endothelial and fibroblast cell adhesion. *Proc. Natl Acad. Sci. USA*, **89**, 2232–2236.

Strydom,D.J., Fett,J.W., Lobb,R.R., Alderman,E.M., Bethune,J.L., Riordan,J.F. and Vallee,B.L. (1985) Amino-acid sequence of human-tumor derived angiogenin. *Biochemistry*, **24**, 5486–5494.

Strynadka,N.C.J., Jensen,S.E., Alzari,P.M. and James,M.N.G. (1996) A potent new mode of β-lactamase inhibition revealed by the 1.7Å X-ray crystallographic structure of the TEM-1–BLIP complex. *Nature Struct. Biol*., **3**, 290–297.

Received on May 13, 1997; revised on June 16, 1997